Indian Journal of Chemistry
Vol. 65, May 2026, pp. 458-474
DOI: 10.56042/ijc.v65i5.25391

Unveiling the mechanism of selected steroids targeting G6PD in gastric cancer through computational approaches

Hung Duc Nguyen
Thai Nguyen University of Education, 24000, Thai Nguyen, Vietnam
E-mail: hungnd@tnue.edu.vn

Received 8 November 2025; accepted (revised) 14 May 2026

Gastric cancer ranks as the fifth leading cause of cancer globally, posing a significant challenge despite extensive research and funding efforts. Medicinal chemists continue to face difficulties in developing practical and durable therapies, particularly due to the heightened reliance of cancer cells on Glucose-6-Phosphate Dehydrogenase (G6PD)-mediated NADPH production compared to normal cells. This study investigates the pharmacokinetics and molecular targets of selected steroids as potential anti-gastric cancer agents. The results demonstrate that these steroids likely induce apoptosis by modulating key signalling pathways, with G6PD inhibition increasing reactive oxygen species and activating caspase-3, while regulating cell survival and proliferation through targets such as ATP1A1 and NOTCH1. Molecular docking analyses with the protein 7E6I reveal that CPD5 exhibits greater stability and better localisation within the 7E6I binding pocket than DHEA. Molecular dynamics simulations over 100 ns further confirm a consistent binding mode, highlighting CPD5's effective inhibition of the protein 7E6I. MMGBSA reveals binding free energies of –5.13 kcal/mol (CPD5-7E6I) *versus* –14.38 kcal/mol (DHEA-7E6I). DFT highlights CPD5's reactivity exceeding DHEA's. ADMET profiling confirms CPD5's non-toxicity, stability, and high absorption. Thus, CPD5 represents a viable candidate for gastric cancer therapy *via* 7E6I inhibition.

Keywords: DFT, *In silico* study, G6PD, Gastric cancer, Molecular target, Steroids

Cancer, characterised by uncontrolled abnormal cell growth and the potential to spread, is a major global health concern. This is a leading cause of death worldwide and a significant contributor to illness and disability. Gastric cancer is the fifth leading cause of cancer in the world, with 968,350 new cases and 659,853 deaths in 2022[1]. Despite significant research efforts and funding, cancer treatment remains a major challenge, and medicinal chemists face ongoing difficulties in developing effective and lasting therapies. Therefore, there is an ongoing and critical need to discover and develop new anticancer drugs that are more effective at killing cancer cells and cause fewer side effects[2,3]. Targeted cancer therapies have indeed become a more prominent and effective treatment option, offering a more precise approach compared to traditional chemotherapy. These therapies focus on specific molecules or pathways involved in cancer cell growth and survival, aiming to minimise damage to healthy cells while maximising the impact on cancerous cells[4,5]. For life to continue, metabolism is essential in every living cell. It encompasses all the chemical reactions that occur within a cell to maintain life, including energy production and the synthesis of new organic material[6]. The pentose phosphate pathway (PPP) plays a critical role in cancer cell metabolism by producing NADPH and ribose-5-phosphate[7,8]. Cancer cells often exhibit altered PPP activity, directing more glucose towards this pathway to meet their increased demands for these molecules. Glucose-6-phosphate dehydrogenase (G6PD) is indeed the rate-limiting enzyme in the oxidative branch of the PPP[9]. Cancer cells often rely more on G6PD-mediated NADPH production than normal cells. This increased dependency arises from the higher metabolic demands and increased oxidative stress that cancer cells experience[10].

The discovery of plant-based antitumor drugs significantly contributes to cancer treatment, receiving significant attention from researchers. Many current cancer treatments rely on compounds derived from plants, and ongoing research explores new plant-derived compounds with potential anticancer properties and investigates their mechanisms of action[11,12]. A previous study of our colleagues on the Chinese traditional medicines led to the isolation of some potential steroids against gastric cancer[13]. However, the compounds have not been thoroughly

investigated at the molecular level, specifically through techniques such as molecular docking, molecular dynamics simulations, and ADMET analysis to better understand their potential as anticancer agents.

Computational drug design is a field that uses computational techniques to identify, design, and optimise potential drug candidates. It leverages computer models and simulations to accelerate and enhance drug discovery by analysing molecular interactions and predicting drug properties before laboratory testing. Computational drug design offers a promising approach to cancer treatment by focusing on both efficacy and reduced side effects, potentially leading to more effective and safer therapies[14,15].

Thus, this study aimed to discover and evaluate the mechanism of selected steroids isolated previously as potential anti-gastric cancer agents. Molecular modelling and ADMET predictions were carried out with molecular target predictions as a potential G6PD inhibitor. The findings provide a foundation for future experimental validation and optimisation of these steroids as effective and safe treatments for gastric cancer, pending further *in vitro* and *in vivo* studies.

Materials and methods

Structural preparation of selected steroids

The list of steroids was collected in the previous study[16]. For detail, twelve selected steroids, including 8*β*-hydroxy-divaricoside (CPD1), 8*β*-hydroxy-17*β*H-divaricoside (CPD2), 17*β*H-sinoside (CPD3), sinogenin (CPD4), sinoside (CPD5), decogenin (CPD6), decoside (CPD7), *ψ*-caudoside (CPD8), caudoside (CPD9), sarmentogenin (CPD10), divaricoside (CPD11), 5*β*-card-20(22)-enolide, 3*β*-(2,6-dideoxy-3-*O*-methyl-*β*-D-xylo-hexopyranosyloxy)-14-hydroxy-11-oxo-6-ol (CPD12), have molecular formulas of $C_{30}H_{46}O_9$, $C_{30}H_{46}O_9$, $C_{30}H_{44}O_9$, $C_{23}H_{32}O_6$, $C_{30}H_{44}O_9$, $C_{23}H_{30}O_6$, $C_{30}H_{42}O_9$, $C_{30}H_{44}O_9$, $C_{30}H_{44}O_9$, $C_{23}H_{34}O_5$, $C_{30}H_{46}O_8$, $C_{30}H_{44}O_8$, and molecular weights of 550.3142, 550.3142, 548.2985, 404.2199, 548.2985, 402.2042, 546.2829, 548.2985, 548.2985, 390.2406, 534.3193, 532.3036 *m/z*, respectively. The DHEA possessing molecular formula of $C_{19}H_{18}O_2$ and molecular weight of 288.2089 was chosen as the positive control (Fig. 1).

Evaluation of the biological activity of selected steroids

The evaluation of the biological activity of selected steroids against gastric cancer cell line (SGC-7901) has been carried out in previous study[16].

Molecular target prediction

Molecular target prediction in drug discovery identifies the specific protein or other molecule in a biological system that a drug interacts with to produce a desired therapeutic effect. This interaction is crucial for understanding how a drug works and for designing new drugs that can effectively target specific diseases[17]. The Similarity Ensemble Approach (SEA) is a computational method used to predict potential molecular targets for phytoconstituents by leveraging the concept of chemical similarity between ligands and known drug targets[18]. The SMILES of each steroid were submitted to the SEA database, with *Homo sapiens* selected as the target species.

Protein-protein interaction network prediction

Protein-protein interaction (PPI) prediction is indeed vital for understanding biological processes, disease mechanisms, and drug development. By identifying how proteins interact, researchers can gain insights into cellular functions, disease pathways, and potential therapeutic targets[19]. According to this benefit, the protein-protein interaction network of selected steroids was predicted using the String database[20], and the human database was selected. Target proteins, previously identified *via* the SEA database, were submitted to STRING, with the *Homo sapiens* database selected to map interactions relevant to human biology.

Biosignaling network prediction

The X2K Web platform (https://maayanlab.cloud/X2K/) was utilised to investigate upstream regulatory networks of steroid target proteins, integrating predictive insights with molecular pathway analysis[21]. X2K combines transcription factor, kinase, and protein-protein interaction data to construct regulatory networks for gene sets derived from SEA and STRING, with *Homo sapiens* specified as the reference species.

Molecular docking

The protocol of molecular docking has been described in the previous study[22]. For details, the 3D structures of all compounds were prepared in .pdb format using Biovia Discovery Studio Visualizer. Only polar hydrogens and the Compute Gasteiger were added, and all torsions were allowed to rotate. The 3D structure of target Glucose-6-phosphate dehydrogenase (G6PD) (protein ID: 7E6I) was retrieved from RCSB Protein Data Bank in .pdb format[23]. The molecular docking of protein and

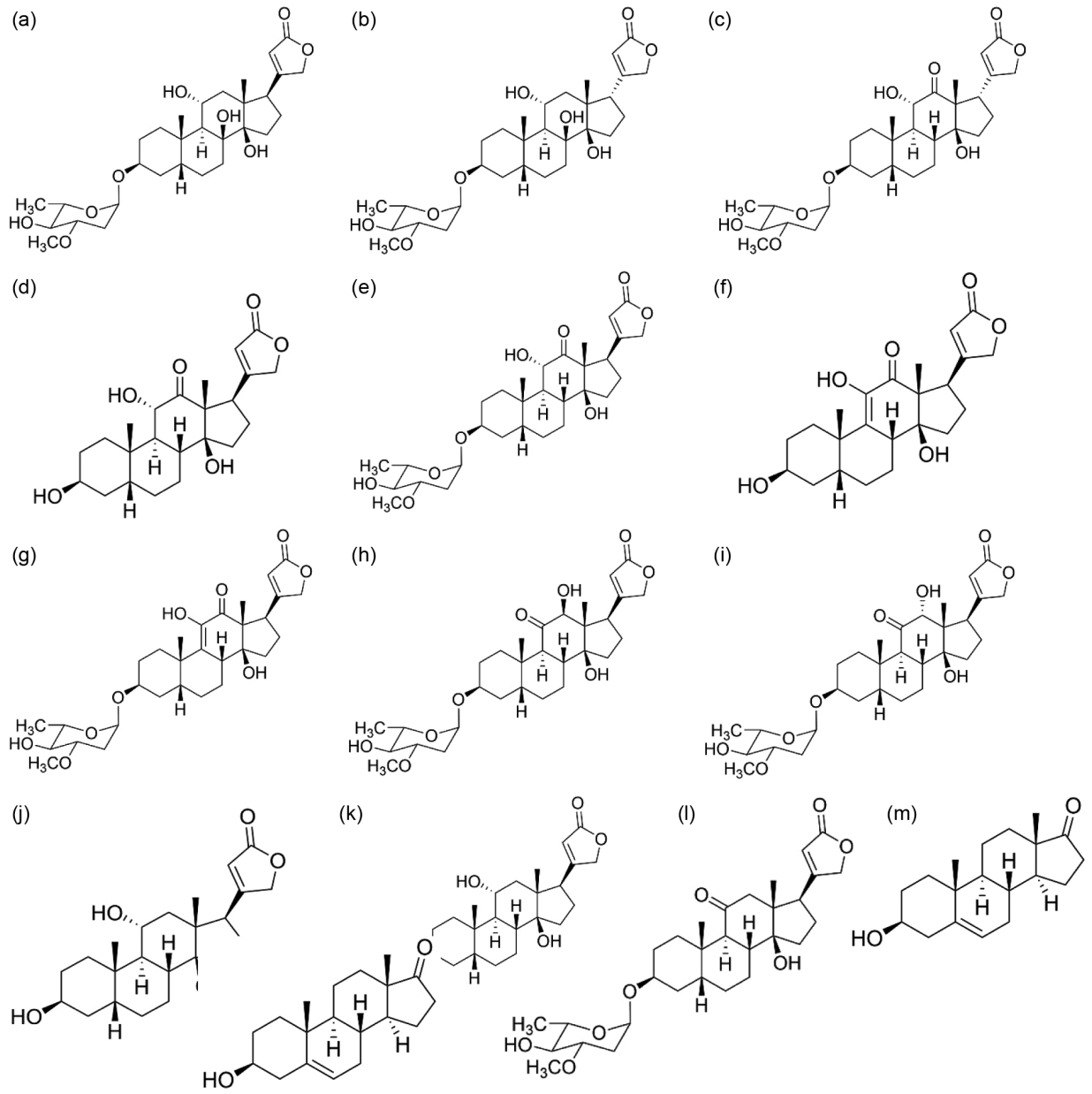

Fig. 1 — Structures of selected steroids. (A) CPD1, (B) CPD2, (C) CPD3, (D) CPD4, (E) CPD5, (F) CPD6, (G) CPD7, (H) CPD8, (I) CPD9, (J) CPD10, (K) CPD11, (L) CPD12, (M) DHEA

ligands was performed using AutoDock Tools. The grid dimensions were set to x = 34, y = 54, z = 58, with a spacing of 0.375 Å between grid points. The docking site coordinates were identified as x = 30.432 Å, y = 79.622 Å, and z = 124.559 Å within the 7E6I protein pocket. The Lamarckian genetic algorithm determined the most energetically favourable ligand-protein binding conformations.

Molecular dynamics simulation

Molecular dynamics simulation for the best-docked confirmation with the 7E6I protein was performed for 100 ns using GROMACS v2024.4 software, using the CHARMM36 force field under physiological-like conditions[24]. The protein was fixed using Swiss-PdbViewer software to avoid missing atoms and residues[25]. Swiss PARAM was used to produce the topologies of ligands[26]. The solvation system utilised a triclinic simulation box tailored to the protein-ligand complex, constructed with the SPC water model. Sodium chloride at a concentration of 0.15 M was incorporated into the system. Energy minimisation and neutralisation for structural optimisation were configured for 50,000 steps. The system was

equilibrated at a temperature of 300 K and a pressure of 1.0 bar. The simulation was executed for 150,000 steps. Molecular dynamics simulation data were evaluated using Grace software (Grace Development Team), analysing parameters including RMSD, RMSF, Rg, and H-bonds.

Drug likeness and ADMET prediction

Computational methods are indeed being used to predict the pharmacological properties of phytochemicals, which are bioactive compounds found in plants. Drug likeness and ADMET (Absorption, Distribution, Metabolism, Excretion, and Toxicity) prediction are crucial in drug discovery and development to identify promising drug candidates early on, minimise costly failures in later stages of development, and optimise compounds for better efficacy and safety. The drug-likeness of selected steroids can be evaluated using pkCSM, a web server that predicts pharmacokinetic and toxicity properties of small molecules. pkCSM utilises graph-based signatures to model compounds and predict ADMET pharmacokinetic properties[27].

Molecular mechanics generalised born surface area (MMGBSA) analysis

The Molecular Mechanics Generalised Born Surface Area (MMGBSA) method represents a computational framework to evaluate the binding free energy between ligands and their corresponding protein targets. Extensively employed in pharmaceutical research and examinations of protein-ligand associations, this technique establishes an equilibrium between exactness and computational demands[28]. It merges molecular dynamics simulations with thermodynamic assessments to ascertain binding free energies. The MMGBSA method, implemented *via* gmx_MMPBSA utilising the charmm36-jul2022.ff force field, was employed to determine the binding free energy for the CPD5-7E6I and DHEA-7E6I complexes. The Generalised Born model enabled the computation of electrostatic solvation energy in a continuum solvent context. Conversely, the non-polar solvation energy was calculated according to the solvent-accessible surface area. Binding free energy figures were derived from 125 snapshots acquired at 80 ps intervals during an 80 ns molecular dynamics simulation (extending from 20 to 100 ns). This procedure generated an averaged binding energy, disclosing the dynamic attributes of protein-ligand interactions and facilitating the appraisal of binding potency and stability in a modelled environment.

Quantum chemistry computation using Density Functional Theory (DFT) method

Density Functional Theory (DFT) is increasingly applied within quantum computing frameworks to investigate the properties of lead compounds, permitting thorough assessment of electronic arrangements, molecular features, and interaction dynamics. The fusion of DFT with quantum computing yields a powerful technique for anticipating and explaining the performance of lead-based materials in multiple settings[29]. Molecular structures of CPD5 and DHEA experienced energy minimisation and full geometry optimisation *via* the ORCA 6.1.0 software suite. Input files originated from Avogadro software, with all energy determinations conducted in the ORCA platform, and output information received visualisation and analysis through IboView v20211019 to augment insight into orbital configurations and molecular geometry[30–33]. DFT calculations occurred at the B3LYP level of theory, incorporating the 6-31G(d,p) basis set to precisely delineate the molecular electronic wave function. Molecular descriptors, encompassing energies of the highest occupied molecular orbital (HOMO) and lowest unoccupied molecular orbital (LUMO), energy gap (ΔE), and reactivity metrics including chemical potential (μ), electronegativity (χ), hardness (η), softness (σ), and electrophilicity index (ω), were derived according to Koopmans' theorem[34,35].

Results and Discussion

Molecular target, protein interaction, and biosignaling network

This study first investigates the molecular targets of selected steroids using SEA to predict protein-ligand interactions based on chemical similarity, STRING to map protein interactions for understanding cellular context, and X2K to identify key signalling pathways regulating apoptosis. These insights then guide subsequent molecular docking, dynamics simulations, and *in silico* ADMET analyses to evaluate their therapeutic potential in gastric cancer, specifically the SGC-7901 cell line. Using the SEA database, key human molecular targets of these steroids, focusing on Glucose-6-Phosphate Dehydrogenase (G6PD), have been identified (Table 1).

For CPD4 and CPD10, G6PD stands out as a significant target with *p*-values of $4.41E^{-35}$ and $7.21E^{-36}$, and MaxTC values of 0.35 and 0.36, respectively, suggesting potent inhibition of the pentose phosphate pathway, which supports NADPH production critical

Table 1 — Molecular target prediction of selected steroids.

S.No.	Compd	Target gene	Target description	*p* value	MTC
1	CPD1	ATP1A1	Sodium/potassium-transporting ATPase subunit alpha-1	2.87E-86	0.56
		SLCO4C1	Solute carrier organic anion transporter family member 4C1	1.87E-60	0.6
		NOTCH1	Neurogenic locus notch homolog protein 1	9.45E-13	0.34
		ATP12A	Potassium-transporting ATPase alpha chain 2	3.82E-11	0.43
		KLF5	Krueppel-like factor 5	2.35E-06	0.44
		PAX8	Paired box protein Pax-8	5.81E-06	0.56
2	CPD2	ATP1A1	Sodium/potassium-transporting ATPase subunit alpha-1	2.87E-86	0.56
		SLCO4C1	Solute carrier organic anion transporter family member 4C1	1.87E-60	0.6
		NOTCH1	Neurogenic locus notch homolog protein 1	9.45E-13	0.34
		ATP12A	Potassium-transporting ATPase alpha chain 2	3.82E-11	0.43
		KLF5	Krueppel-like factor 5	2.35E-06	0.44
		PAX8	Paired box protein Pax-8	5.81E-06	0.56
3	CPD3	ATP1A1	Sodium/potassium-transporting ATPase subunit alpha-1	5.77E-97	0.61
		SLCO4C1	Solute carrier organic anion transporter family member 4C1	6.45E-64	0.61
		NOTCH1	Neurogenic locus notch homolog protein 1	9.99E-15	0.34
		KLF5	Krueppel-like factor 5	3.87E-06	0.42
		PAX8	Paired box protein Pax-8	3.88E-06	0.61
4	CPD4	ATP1A1	Sodium/potassium-transporting ATPase subunit alpha-1	1.45E-69	0.46
		ATP12A	Potassium-transporting ATPase alpha chain 2	3.60E-69	0.66
		SLCO4C1	Solute carrier organic anion transporter family member 4C1	1.70E-67	0.65
		G6PD	Glucose-6-phosphate 1-dehydrogenase	4.41E-35	0.35
		SERPINA6	Corticosteroid-binding globulin	4.33E-21	0.35
		NOTCH1	Neurogenic locus notch homolog protein 1	2.94E-17	0.41
		SHBG	Sex hormone-binding globulin	1.36E-11	0.35
		GABRD	Gamma-aminobutyric acid receptor subunit delta	2.27E-09	0.35
		GPBAR1	G-protein coupled bile acid receptor 1	1.21E-08	0.35
		PAX8	Paired box protein Pax-8	3.68E-06	0.66
5	CPD5	ATP1A1	Sodium/potassium-transporting ATPase subunit alpha-1	5.77E-97	0.61
		SLCO4C1	Solute carrier organic anion transporter family member 4C1	6.45E-64	0.61
		ATP12A	Potassium-transporting ATPase alpha chain 2	1.36E-25	0.44
		NOTCH1	Neurogenic locus notch homolog protein 1	9.99E-15	0.34
		KLF5	Krueppel-like factor 5	3.87E-06	0.42
		PAX8	Paired box protein Pax-8	3.88E-06	0.61
6	CPD6	SLCO4C1	Solute carrier organic anion transporter family member 4C1	1.12E-55	0.53
		ATP12A	Potassium-transporting ATPase alpha chain 2	6.54E-31	0.54
		ATP1A1	Sodium/potassium-transporting ATPase subunit alpha-1	7.95E-20	0.38
		NOTCH1	Neurogenic locus notch homolog protein 1	3.89E-15	0.36
		SERPINA6	Corticosteroid-binding globulin	1.47E-09	0.29
		SLCO4C1	Solute carrier organic anion transporter family member 4C1	1.12E-55	0.53
7	CPD7	ATP1A1	Sodium/potassium-transporting ATPase subunit alpha-1	2.04E-83	0.55
		SLCO4C1	Solute carrier organic anion transporter family member 4C1	3.60E-55	0.55
		NOTCH1	Neurogenic locus notch homolog protein 1	7.87E-12	0.32
		ATP12A	Potassium-transporting ATPase alpha chain 2	1.57E-09	0.36

(*Contd.*)

Table 1 — Molecular target prediction of selected steroids.

S.No.	Compd	Target gene	Target description	*p* value	MTC
8	CPD8	ATP1A1	Sodium/potassium-transporting ATPase subunit alpha-1	1.44E-103	0.68
		SLCO4C1	Solute carrier organic anion transporter family member 4C1	2.45E-68	0.63
		ATP12A	Potassium-transporting ATPase alpha chain 2	2.91E-25	0.44
		NOTCH1	Neurogenic locus notch homolog protein 1	1.68E-14	0.34
		PAX8	Paired box protein Pax-8	5.85E-06	0.68
9	CPD9	ATP1A1	Sodium/potassium-transporting ATPase subunit alpha-1	1.44E-103	0.68
		SLCO4C1	Solute carrier organic anion transporter family member 4C1	2.45E-68	0.63
		ATP12A	Potassium-transporting ATPase alpha chain 2	2.91E-25	0.44
		NOTCH1	Neurogenic locus notch homolog protein 1	1.68E-14	0.34
		PAX8	Paired box protein Pax-8	5.85E-06	0.68
10	CPD10	ATP12A	Potassium-transporting ATPase alpha chain 2	1.33E-77	0.75
		SLCO4C1	Solute carrier organic anion transporter family member 4C1	8.87E-71	0.66
		ATP1A1	Sodium/potassium-transporting ATPase subunit alpha-1	8.53E-67	0.45
		G6PD	Glucose-6-phosphate 1-dehydrogenase	7.21E-36	0.36
		SERPINA6	Corticosteroid-binding globulin	1.06E-21	0.35
		NOTCH1	Neurogenic locus notch homolog protein 1	5.79E-19	0.46
		SHBG	Sex hormone-binding globulin	7.53E-12	0.35
		GPBAR1	G-protein coupled bile acid receptor 1	3.12E-11	0.35
		KLF5	Krueppel-like factor 5	6.30E-09	0.49
		PAX8	Paired box protein Pax-8	1.42E-07	0.75
11	CPD11	ATP1A1	Sodium/potassium-transporting ATPase subunit alpha-1	2.82E-96	0.61
		SLCO4C1	Solute carrier organic anion transporter family member 4C1	1.47E-67	0.68
		ATP12A	Potassium-transporting ATPase alpha chain 2	7.18E-34	0.49
		NOTCH1	Neurogenic locus notch homolog protein 1	2.22E-16	0.39
		KLF5	Krueppel-like factor 5	2.48E-07	0.53
		PAX8	Paired box protein Pax-8	8.92E-07	0.73
12	CPD12	ATP1A1	Sodium/potassium-transporting ATPase subunit alpha-1	3.10E-93	0.61
		SLCO4C1	Solute carrier organic anion transporter family member 4C1	9.53E-67	0.67
		ATP12A	Potassium-transporting ATPase alpha chain 2	2.69E-26	0.49
		NOTCH1	Neurogenic locus notch homolog protein 1	2.22E-16	0.39
		PAX8	Paired box protein Pax-8	2.11E-06	0.61
		KLF5	Krueppel-like factor 5	2.16E-06	0.43

for cancer cell survival. Additional notable targets include ATP1A1 (*p*-value: $1.44E^{-103}$, MaxTC: 0.68), SLCO4C1 (*p*-value: $2.45E^{-68}$, MaxTC: 0.63), ATP12A (*p*-value: $1.33E^{-77}$, MaxTC: 0.75), and NOTCH1 (*p*-value: $1.68E^{-14}$, MaxTC: 0.34), indicating a multifaceted mechanism involving oxidative stress from G6PD inhibition, ion dysregulation from ATP1A1/ATP12A inhibition, and signaling modulation by NOTCH1. These targets contribute to increased reactive oxygen species (ROS), a critical precursor to caspase-3 activation and apoptosis in SGC-7901 cells.

Further analysis with the STRING network, centered on G6PD, revealed direct interactions with proteins such as ATP1A1, SLCO4C1, ATP12A, and NOTCH1, as visualised in Fig. 2. These interactions indicate G6PD's role in modulating oxidative stress (*via* ATP1A1, ATP12A) and cellular signalling (NOTCH1), which can contribute to apoptosis in SGC-7901 cells. The presence of ATP1A1 and ATP12A, both Na^+/K^+-ATPase subunits, highlights a mechanism of ion dysregulation and reactive oxygen species (ROS) accumulation, indirectly engaging caspase-3 through stress-induced pathways such as p38 MAPK. Indirect interactions with SLCO4C1 suggest a role in compound transport, potentially enhancing the intracellular accumulation of selected steroids. At the same time, NOTCH1 modulation may suppress pro-survival signalling, further supporting a pro-apoptotic environment. For compounds targeting additional proteins like KLF5 and PAX8, regulatory

transcription and cellular differentiation roles may indirectly bolster apoptosis by altering gene expression profiles.

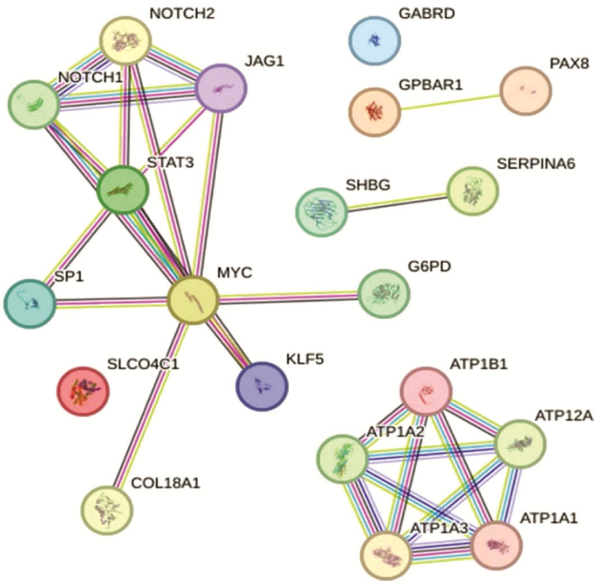

Fig. 2 — Protein-protein interactions of molecular targets of selected steroids

Additionally, X2K analysis provided a comprehensive network, identifying key kinases including MAPK14 (p38α), MAPK8 (JNK1), and MAPK3 (ERK1) in Fig. 3, which are implicated in stress signalling and apoptosis regulation. MAPK14 and MAPK8 play critical roles in triggering pro-apoptotic pathways when activated by oxidative stress induced by G6PD inhibition. At the same time, MAPK3 modulates cell survival and differentiation, potentially enhancing apoptosis under stress conditions in SGC-7901 cells. X2K further expanded the network with additional kinases such as CHEK2 and CSNK2A1, as shown in Fig. 4A, which support DNA damage response and stress signalling, leading to caspase-3 activation. Transcription factors identified in Fig. 3 include NFE2L2 (implied from oxidative stress targets), E2F1, and STAT3, while Fig. 4B highlighted additional factors such as SMAD4. NFE2L2 regulates oxidative stress responses, counteracting ROS accumulation from G6PD inhibition, while E2F1 and STAT3 enhance the expression of pro-apoptotic genes such as BAX and PUMA through p53 and inflammatory pathways.

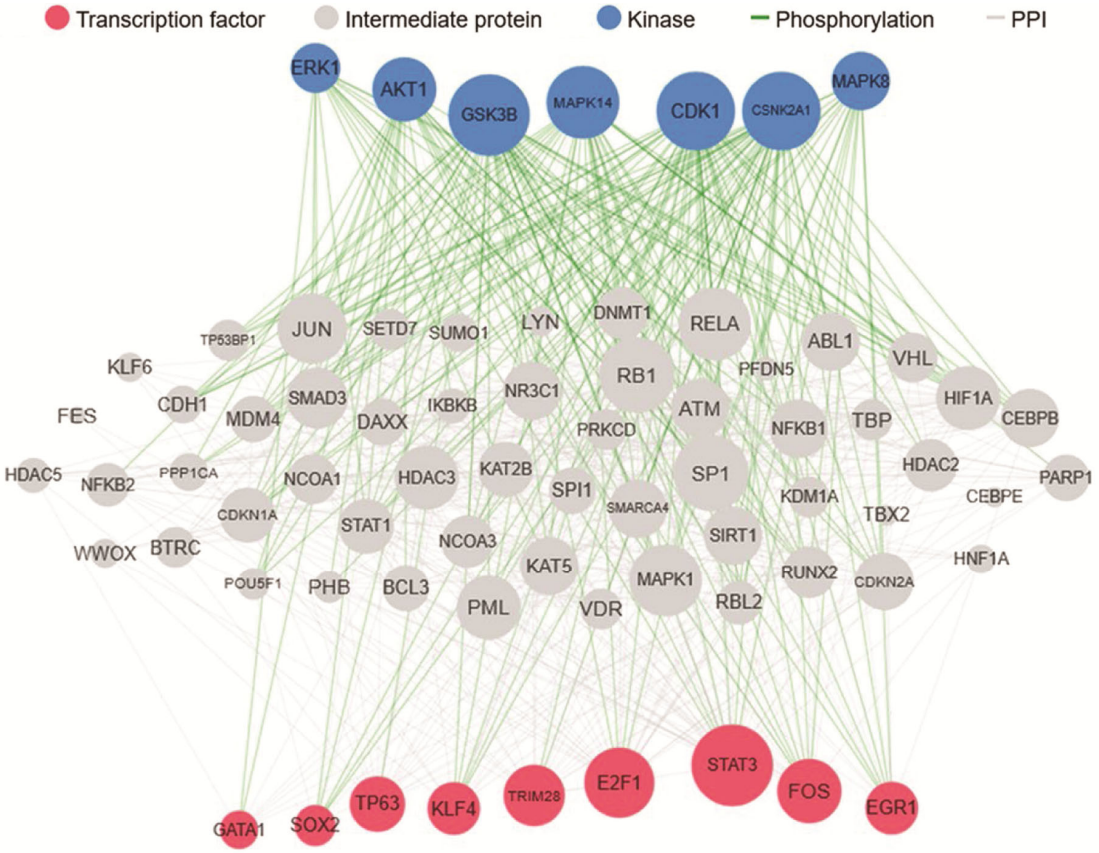

Fig. 3 — Network of kinases and transcription factors linked to molecular targets of selected steroids

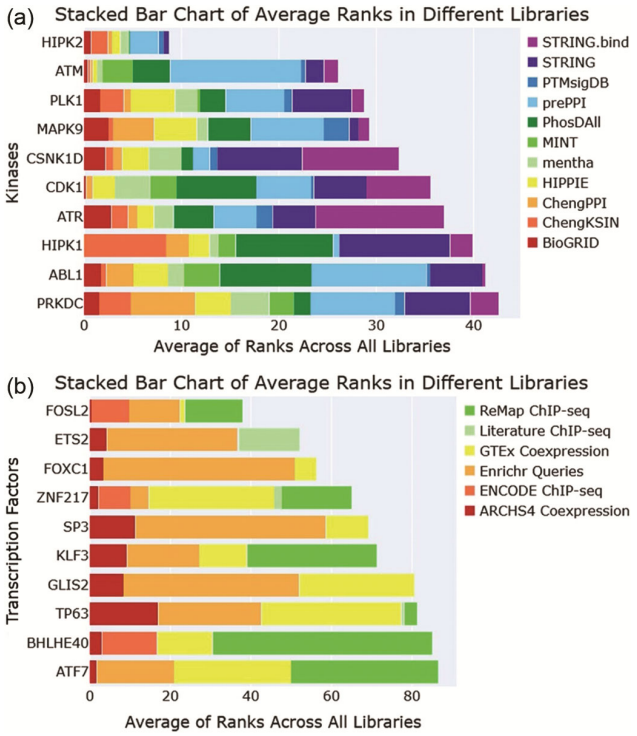

Fig. 4 — Selected steroids associated with kinases (A) and transcription factors (B) average rank across biological libraries

SMAD4 further modulates TGF-β signalling, supporting caspase-3 activation (Fig. 3, Fig. 4).

This evidence strongly supports the conclusion that selected steroids can induce apoptosis in gastric cancer (SGC-7901) through caspase-3 activation. The SEA analysis identified upstream targets, with G6PD as a primary focus for CPD4 and CPD10 (p-values: $4.41E^{-35}$ and $7.21E^{-36}$, MaxTC: 0.35 and 0.36), initiating oxidative stress cascades, as detailed in Table 1; STRING mapped direct interactions of G6PD with ATP1A1, SLCO4C1, ATP12A, and NOTCH1, influencing these pathways, as visualized in Fig. 2; and X2K delineated the pathways (MAPK14, MAPK8, NFE2L2, E2F1, BAX, PUMA) leading to pro-apoptotic gene expression.

Docking analysis

Before docking ligands with the 7E6I protein, the first step was to identify the active sites in the 7E6I pocket. Visualization structure of 7E6I protein using Biovia Discovery Studio Visualizer revealed the active sites involved in inhibiting the protein, which included LYS153, HIS183, TYR184, GLU221, ASP240, HIS245, LYS339, GLN373, THR395, GLU397, and ASP399 (Fig. 5A). The redocking of the co-crystalized ligand was performed, and the

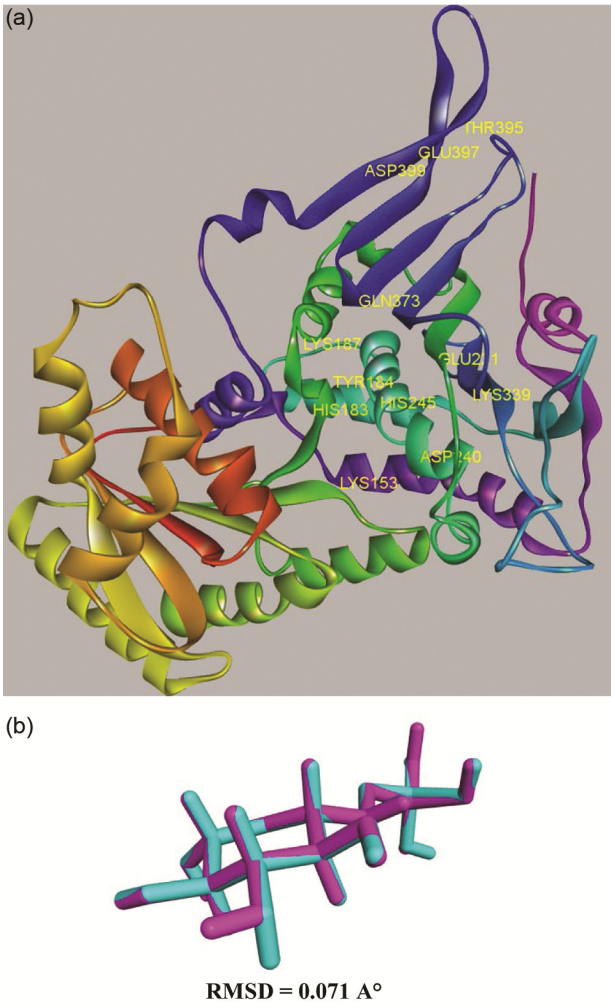

Fig. 5 — The active sites in the protein 7E6I (A) and the superposition of the docked and original ligands validating molecular docking protocol (violet = original, cyan = docked) (B)

validity of the docking protocol was confirmed in Fig. 5B. The RMSD value of 0.071 Å, along with the superposition of the original and docked ligands, verifies the accuracy and precision of the docking protocol. A docking procedure is deemed reliable in molecular docking validation when the RMSD value is below 2 Å[36].

The selected steroids were evaluated through molecular docking against the 7E6I protein, using DHEA as the reference. The docked complexes were assessed based on their minimum binding energy values (kcal/mol). The interactions of the ligands within the binding pockets of the 7E6I protein are presented in Table 2. Key amino acid residues and their positions in the ligand-binding sites were determined. The interactions between the protein and ligands, including hydrogen bonds, Van der Waals forces, and hydrophobic interactions, are illustrated in Fig. 6. A

Table 2 — The interactions between the docked ligands and the protein 7E6I

S.No.	Docked ligands	Binding energy (kcal/mol)	Hydrogen bond interaction	Van der Waals interaction	Hydrophobic interaction
1	CPD1	–6.75	Lys24, Asp240	Lys153, Tyr184, Lys187, Phe219, Arg228, Tyr231, Phe232, Ile235, His245, Lys339, Ala414, Tyr415	His183, Gln373
2	CPD2	–6.40	Lys24, Lys187, Asp240, Lys339, Tyr415	Lys153, Tyr184, Phe219, Glu221, Phe223, Arg228, Tyr231, Phe232, Ile235, His245, Gln373, Ala414	His183
3	CPD3	–6.63	Lys187, Glu221, Arg228, Lys339, Gln373	His183, Tyr184, Phe219, Phe223, Thr225, Tyr231, Phe232, Asp240, His245, Val346	Arg228, Ile235
4	CPD4	–6.81	Lys153, His283, Arg228, Asp240, His245	Glu152, Pro154, Ile181, Asp182, Tyr231, Phe232, Tyr415	Ile235
5	CPD5	–7.85	Lys220, Glu221, Asp240, Lys345, Gln373	Lys153, Tyr184, Lys187, Phe223, Thr225, Arg228, Tyr231, Phe232, Ile235, Val241, Lys339, Val346	His183, Phe219, Glu221, His245
6	CPD6	–7.10	Lys187, Gly224, Asp240	Lys153, His183, Tyr184, Phe219, Glu221, Phe223, Thr225, Phe232, Val241, His245, Lys339, Gln373	Arg228
7	CPD7	–6.00	His183, Lys187, Glu221, Arg228, Lys339, Gln373	Lys24, Tyr184, Phe223, Thr225, Tyr231, Phe232, Asp240	Arg228, Ile235
8	CPD8	–6.99	Lys187, Glu221, Arg228, Lys339, Gln373	Lys24, His183, Tyr184, Phe219, Phe223, Thr225, Tyr231, Phe232, Asp240, His245	Arg228, Ile235
9	CPD9	–6.42	His183, Lys187, Glu221, Arg228, Lys339, Gln373	Lys24, Tyr184, Phe223, Thr225, Tyr231, Phe232, Asp240	Arg228, Ile235
10	CPD10	–6.83	His187, Arg228, Asp240	Lys153, His183, Tyr184, Phe219, Glu221, Phe223, Thr225, Tyr231, Val241, His245, Lys339, Gln373	Arg228, Phe232
11	CPD11	–6.75	His183, Glu221, Arg228, Lys339, Gln373	Lys24, Tyr184, Lys187, Phe219, Phe223, Thr225, Tyr231, Phe232, Asp240	His183, Arg228, Ile235
12	CPD12	–6.38	Lys24, Lys187, Arg228	Tyr184, Phe219, Glu221, Phe223, Thr225, Phe232, Asp240, Lys339, Gln373, Glu413, Ala414, Tyr415	His183
13	DHEA	–6.95	Gly224	Phe223, Thr225, Glu226, Tyr231, Ile235, Asp240, Lys339	Arg228, Phe232

detailed description of each molecular interaction with the 7E6I protein's amino acids follows.

A comparison of the interactions between selected steroids and DHEA reveals that CPD2, CPD5, CPD6, and CPD10 interact with the most active sites of the protein 7E6I. All selected steroids exhibited hydrogen bonds, Van der Waals, and hydrophobic interactions, in which Van der Waals interactions significantly contribute to the stability and binding affinity of protein-ligand complexes[37,38]. In contrast, hydrogen bonds and hydrophobic interactions play significant roles in guiding ligand binding and determining binding affinity. Hydrogen bonds are important for the specificity of interactions, while hydrophobic interactions are often the primary driving force for complex formation[39,40]. Among the compounds analyzed, CPD5 exhibited the most stable binding energy with the protein 7E6I at –7.85 kcal/mol, surpassing CPD1 (–6.75 kcal/mol), CPD2 (–6.40 kcal/mol), CPD3 (–6.63 kcal/mol), CPD4 (–6.81 kcal/mol), CPD6 (–7.10 kcal/mol), CPD7 (–6.00 kcal/mol), CPD8 (–6.99 kcal/mol), CPD9 (–6.42 kcal/mol), CPD10 (–6.83 kcal/mol), CPD11 (–6.75 kcal/mol), CPD12 (–6.38 kcal/mol), and the comparative reference DHEA (–6.95 kcal/mol). The negative binding energy values indicate strong and stable interactions between the ligands and the G6PD active site, suggesting that CPD5 is particularly well localised within the protein's binding pocket. This stability is further supported by the presence of eight hydrogen bonds (with residues Lys220, Glu221, Asp240, Lys345, Gln373) and a diverse range of van der Waals (Lys153, Tyr184, Lys187, Phe223, Thr225, Arg228, Tyr231, Phe232, Ile235, Val241, Lys339,

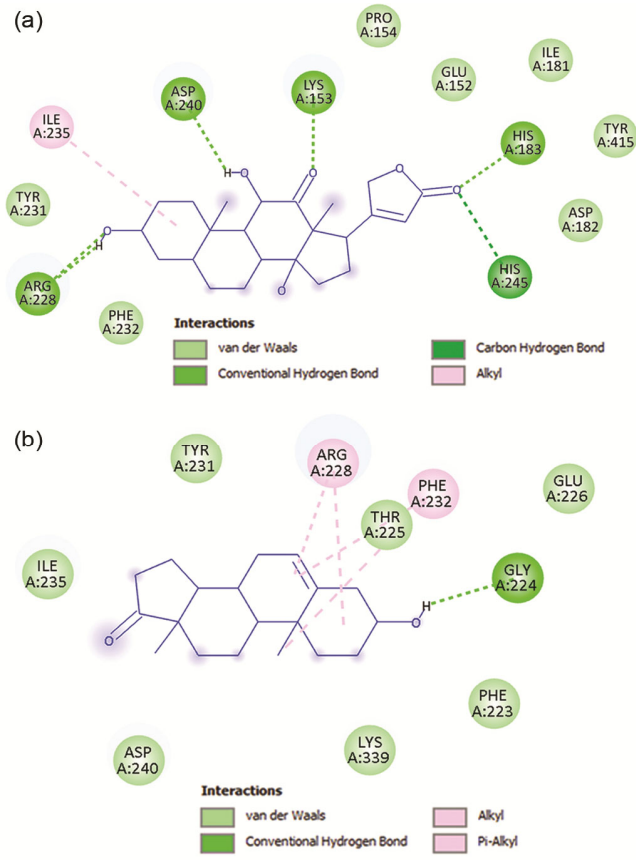

Fig. 6 — Modelling interaction diagram of CPD5 (A) and DHEA (B) with the protein 7E6I.

Val346) and hydrophobic interactions (His183, Phe219, Glu221, His245), indicating a robust binding profile. Given these promising docking results, it is highly interesting to conduct molecular dynamics studies to further elucidate the ligand dynamics and stability of the CPD5-7E6I complex within the target protein's binding pocket, compared to those of the DHEA-7E6I complex.

Molecular Dynamics Simulation

In this study, a molecular dynamics simulation analysis was carried out on the complexes CPD5-7E6I and DHEA-7E6I to examine the root mean square deviation (RMSD), the root mean square fluctuation (RMSF) of each residue, the radius of gyration (Rg) in the given structure, and the number of hydrogen bonds (H-bonds) in each frame over time. As a result, the total energy was calculated as –981,248 kJ/mol for CPD5 and –981,391 kJ/mol for DHEA. The potential values were calculated as –1,219,840 kJ/mol for CPD5 and 1,219,870 kJ/mol for DHEA. The system was equilibrated at a temperature of 300K.

In molecular dynamics simulations, the RMSD is an important metric for assessing the stability and convergence of a simulation. It quantifies the average distance between atomic positions in a simulated and reference structures, often the starting or known experimental structures. Analysing RMSD helps determine if the simulated system has reached a stable state or if further simulation time is needed. Lower RMSD (Root Mean Square Deviation) values indicate that the structures of the simulated molecules are more similar, suggesting a more stable or consistent simulation. Conversely, higher RMSD values indicate greater structural variation or instability, meaning the simulated structures deviate more from each other[41]. The RMSD values for the CPD5-7E6I and DHEA-7E6I complexes ranged from 0.30 to 0.50 nm over a 100 ns period, with an average of 0.38 nm for the remainder of the simulation (Fig. 7A). This suggests that both CPD5 and the reference compound DHEA bound stably to the protein 7E6I, with minor conformational fluctuations indicating a well-equilibrated system. The slightly lower average RMSD for CPD5 (0.35 nm) compared to DHEA (0.40 nm) further highlights the potential stability of the CPD5-7E6I complex, consistent with its higher docking binding energy of –7.85 kcal/mol *versus* –6.95 kcal/mol for DHEA.

The RMSF is a key indicator for assessing the flexibility and dynamics of biomolecules. It measures the average deviation of atomic positions from their mean over time, highlighting regions of greater flexibility or rigidity during the simulation. High RMSF values indicate highly flexible regions, while low values suggest rigidity[42]. Fig. 7B demonstrates that the RMSF values for regions at residues 0-200 of G6PD exhibit significant flexibility, suggesting high conformational variability. This flexibility may be attributed to the distance of these residues from the active binding sites, particularly the $NADP^+$-binding site (around residues 205, 487) and the G6P-binding site (around residues 178, 239), which are less constrained by ligand interactions. On the other hand, the key amino acid residues within the binding pockets that interact more stably with the divaricoside compound, such as Lys205, Arg487, His178, and Glu239, display relatively low RMSF values, indicating enhanced stability. The regions around residues 150-300, encompassing the binding pocket, show particularly low RMSF values, reflecting good structural rigidity and consistent interactions with the ligand throughout the 100 ns simulation.

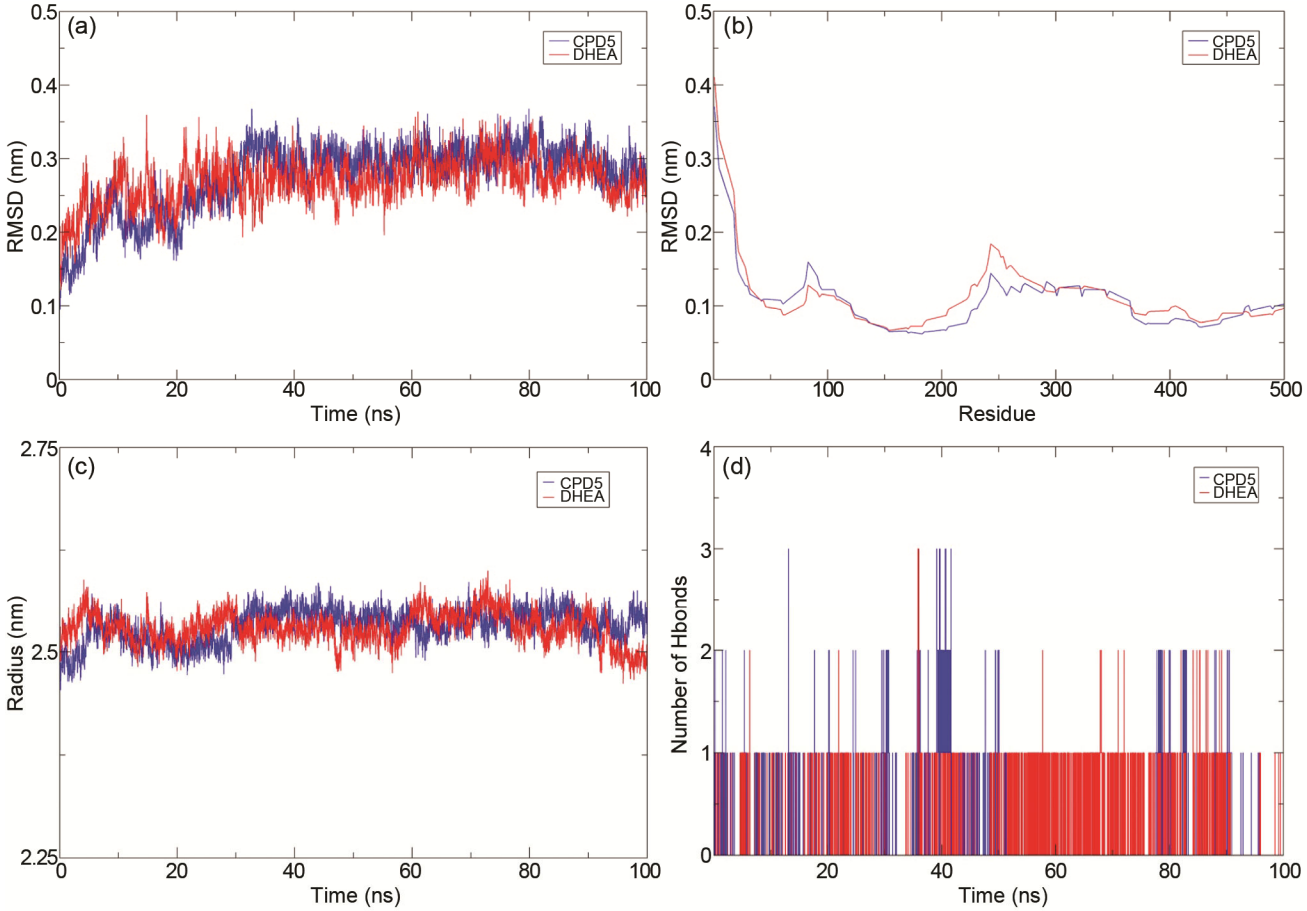

Fig. 7 — Results of MD simulation for the bindings of CPD5 (blue) and DHEA (red) with the protein 7E6I. (A) RMSD, (B) RMSF, (C) The radius of gyration (Rg), (D) The number of hydrogen bonds (H-bonds)

The Rg is a valuable metric for assessing protein structure compactness in molecular dynamics simulations. It's calculated as the root mean square distance of all atoms in a protein from its centre of mass, quantifying how spread out or compact a protein's structure is. Smaller Rg values indicate more compact, globular structures, while larger Rg values suggest more extended or flexible conformations[43]. The analysis of the Rg values for each complex is shown in Fig. 7C. The Rg values for all complexes were consistently stable, ranging from 1.7 to 1.8 nm throughout the 100 ns simulation, confirming that the complex exhibits a relatively compact protein structure. This stability suggests that the binding of divaricoside to the active sites of 7E6I, particularly the $NADP^+$-binding site (around residues 205, 487) and the G6P-binding site (around residues 178, 239), does not significantly alter the global conformation of the protein, maintaining its structural integrity during the simulation.

Hydrogen bonds stabilise interactions between a ligand molecule and a protein target. They contribute significantly to the interaction's overall binding affinity and specificity, guiding the ligand to its correct binding site on the protein. These bonds are directional, and their geometry plays a vital role in the strength and stability of the interaction[44]. The results showed that H-bonds were observed throughout the simulation, with 2-5 hydrogen bonds consistently formed in the CPD5-7E6I complex and 1-3 hydrogen bonds consistently formed in the DHEA-7E6I complex, indicating stable interactions within the binding pocket. These hydrogen bonds primarily involve key residues such as Lys205, Arg487, His178, and Glu239, located in the $NADP^+$-binding site and G6P-binding site of 7E6I. The higher number of H-bonds (2-5) in the CPD5-7E6I complex suggests that CPD5 remained more stably anchored within the active sites compared to DHEA, which exhibited a lower range (1-3) of H-bonds. These findings indicate

that CPD5 may form a stronger and more consistent interaction with 7E6I throughout the 100 ns simulation, potentially enhancing its inhibitory effect on the pentose phosphate pathway in SGC-7901 cells (Fig. 7D).

The molecular dynamics simulation results demonstrate a sustained inhibition mode and stable binding interactions across all simulations, as evidenced by RMSD values ranging from 0.35 to 0.55 nm (average 0.4 nm over 100 ns), consistent Rg values of 1.7 to 1.8 nm indicating compact protein structures, and dynamic hydrogen bond formations (2-5 for the CPD5-7E6I and 1-3 for the DHEA-7E6I complexes). These findings collectively confirm the robust and stable binding of selected steroids, particularly CPD5, to the protein 7E6I throughout the simulation, underscoring their potential as effective inhibitors of the pentose phosphate pathway, leading to increased reactive oxygen species (ROS) and caspase-3 activation in SGC-7901 gastric cancer therapy. To further evaluate the therapeutic viability of these steroids, the next section will focus on *in silico* ADMET analyses to assess their pharmacokinetic properties and safety profiles.

Drug likeness and ADMET prediction

ADMET predictions were conducted using the pkCSM databases to assess the oral bioavailability of CPD5 in comparison to DHEA[45], with detailed results provided in Table 3. In ADMET, absorption is how a drug enters the body and reaches its target. It's the process by which a drug moves from the site of administration into the bloodstream, and factors like lipophilicity, solubility, and the presence of transporters significantly influence this process. Understanding absorption is key to predicting a drug's bioavailability and identifying the most effective delivery method[46]. Regarding the percentage of absorption by the human intestines, a value less than 30% indicates low absorption[47]. CPD5 presented an absorption value of 91.144%, which guarantees a

Table 3 — Predicted ADMET properties of CPD5 and DHEA

ADMET properties	Unit	CPD5	DHEA
Water Solubility	(Log mol/L)	–4.976	–4.504
Caco2 permeability	(Log Papp in 10^{-6} cm/s)	0.758	1.665
Intestinal absorption (Human)	(% Absorbed)	91.144	94.629
Skin permeability	(Log Kp)	–3.527	–2.951
P-glycoprotein substrate	Yes/No	Yes	No
P-glycoprotein I inhibitor	Yes/No	Yes	Yes
P-glycoprotein II inhibitor	Yes/No	Yes	No
VDss	(Log L/kg)	–0.199	0.519
Fraction unbound (human)	(Fu)	0.169	0.2
BBB permeability	(Log BB)	–1.204	0.134
CNS permeability	(Log PS)	–3.129	–2.628
CYP2D6 substrate	Yes/No	No	No
CYP3A4 substrate	Yes/No	Yes	Yes
CYP1A2 inhibitor	Yes/No	No	No
CYP2C19 inhibitor	Yes/No	No	No
CYP2C9 inhibitor	Yes/No	No	No
CYP2D6 inhibitor	Yes/No	No	No
CYP3A4 inhibitor	Yes/No	No	No
Total clearance	(Log mL/min/kg)	0.54	0.936
Renal OCT2 substrate	Yes/No	No	Yes
AMES toxicity	Yes/No	No	No
Max. tolerated dose (human)	(Log mg/kg/day)	–1.345	–0.413
hERG I inhibitor	Yes/No	No	No
hERG II inhibitor	Yes/No	No	Yes
Oral rat acute toxicity (LD50)	(mol/kg)	2.944	1.759
Oral rat chronic toxicity (LOAEL)	(Log mg/kg_bw/day)	1.801	1.82
Hepatotoxicity	Yes/No	No	No
Skin sensation	Yes/No	No	No
Tetrahymena pyriformis toxicity	(Log ug/L)	0.286	1.09
Minnow toxicity	(Log mM)	2.203	1

good absorption by the human intestine, slightly lower than the DHEA compound at 94.629%. Both values significantly exceed the low absorption threshold, suggesting excellent gastrointestinal bioavailability for both steroids, with DHEA demonstrating a marginally superior absorption profile.

In drug development, distribution refers to how a drug moves throughout the body after absorption, reaching different tissues and organs *via* the bloodstream. Understanding a drug's distribution is crucial because it dictates where it accumulates, how it interacts with its target, and ultimately, its efficacy and potential toxicity. Regarding distribution indicators, a high volume of distribution at steady state (VDss), typically considered greater than 0.45, indicates that a drug is widely distributed throughout the body and not just confined to the bloodstream. This means the drug can reach various tissues and organs. Conversely, a low VDss suggests the drug primarily remains in the plasma[48]. The standard value for blood-brain barrier (BBB) permeability is good if its value is more than 0.3, and poor if LogBB < –1[49]. For the CNS index, compounds with LogPS > –2 can penetrate the central nervous system (CNS). In contrast, compounds with LogPS < –3 are considered incapable of penetrating the CNS[50]. The distribution indices reported by CPD5 indicated a lower distribution capacity, with a VDss of –0.199 log L/kg, suggesting a limited volume of distribution, compared to DHEA, which exhibited a higher VDss of 0.519 log L/kg, indicating a better distribution profile. CPD5 showed a LogBB of –1.204 for BBB permeability, indicating poor permeability, while DHEA demonstrated good permeability with a LogBB of 0.134. Regarding CNS permeability, both compounds exhibited LogPS values (CPD5: –3.129, DHEA: –2.628) below the threshold of –2, suggesting that neither CPD5 nor DHEA can effectively penetrate the CNS. The fraction unbound (Fu) values, with CPD5 at 0.169 and DHEA at 0.2, indicate moderate protein binding, with DHEA showing a slightly higher unbound fraction, potentially enhancing its distribution efficiency

Metabolism refers to the process by which the body breaks down a drug or other chemical compound. It's a crucial aspect of ADMET because it influences how a drug behaves in the body, impacting its efficacy, duration of action, and potential for toxicity. Cytochrome P450 (CYP) enzymes are a large and diverse family of enzymes that primarily metabolise drugs, toxins, and various endogenous substances. These enzymes are crucial for the detoxification of foreign compounds and play a significant role in the body's overall metabolic processes[51]. Inhibitors of CYP enzymes can alter drug metabolism, potentially reversing the drug's intended effects[52]. As a result, assessing the capacity of compounds to inhibit CYP enzymes is vital. To date, 18 different CYP families have been identified in humans, but only CYP1, CYP2, CYP3, and CYP4 are involved in drug metabolism. Among these, the enzymes CYP1A2, CYP2C9, CYP2C19, CYP2D6, and CYP3A4 account for the biotransformation of more than 90% of drugs during their initial metabolism phase[53]. The isoforms CYP2D6 and CYP3A4 are primarily responsible for this process[54]. From the obtained results of the metabolism properties, both CPD5 and DHEA are substrates for CYP3A4, but neither acts as an inhibitor for CYP1A2, 2C19, 2C9, 2D6, or 3A4. Additionally, neither compound is a substrate for CYP2D6. This indicates that the metabolism of CPD5 and DHEA as drugs is primarily mediated by CYP3A4, suggesting a stable metabolic profile without significant inhibition, allowing them to reach their therapeutic target before being oxidised and potentially excreted.

The liver and kidneys are the primary organs involved in drug elimination, with the liver metabolising drugs and the kidneys primarily responsible for excretion. While the liver metabolises drugs and excretes them *via* bile, the kidneys excrete unmetabolized drugs and metabolites in the urine[55]. In ADMET, total clearance refers to the volume of plasma cleared of a drug per unit of time. It indicates the body's efficiency in eliminating the drug, encompassing renal and non-renal pathways[56]. The excretion property was evaluated in this study to determine the level of stability of CPD5 and DHEA as potential drugs in the body before their excretion. The predictive values of this index showed that the total clearance index of CPD5 is 0.54 log mL/min/kg, which is lower than the total clearance index of DHEA at 0.936 log mL/min/kg, suggesting that CPD5 may persist in the body better than DHEA. This greater stability of CPD5, further supported by its non-substrate status for renal OCT2 compared to DHEA, enhances its efficacy as a 7E6I inhibitor at lower doses, offering a significant advantage for sustained therapeutic action in gastric cancer therapy.

ADMET studies, including toxicity assessments, are essential for identifying potential risks early in the drug development process, which can save significant resources and prevent harm. Understanding a drug's

toxicity profile helps determine its suitability for further development, avoiding late-stage failures and ensuring patient safety. The Ames test is a widely used, cost-effective bacterial assay that evaluates the mutagenic potential of chemical compounds. It helps determine if a substance can cause mutations in bacteria, which can indicate a potential carcinogenic risk[57]. Therefore, the AMES test was applied to assess CPD5 and DHEA. As a result, these compounds demonstrated non-toxic properties.

Based on the *in silico* ADMET evaluation results for CPD5 and DHEA, it can be concluded that CPD5 satisfies key pharmacokinetic criteria, demonstrating non-toxicity, superior stability with lower clearance, and high intestinal absorption. As a result, CPD5 shows potential as a future drug for treating gastric cancer by inducing apoptosis through 7E6I inhibition. Furthermore, CPD5 could be a foundation for designing new compounds with enhanced biological activities, improved safety profiles, and novel therapeutic applications in cancer therapy.

Free binding energy (MMGBSA) analysis

The binding free energies for ligand-protein complexes were calculated using the MMGBSA method, implemented *via* the gmx_MMPBSA software and the charmm36-jul2022.ff force field. The Molecular Mechanics/Generalised Born Surface Area (MM-GBSA) analysis incorporated frames derived from molecular dynamics simulations spanning 100 ns. The binding free energy (ΔG_binding) in the ligand-protein complexes is expressed as ΔG_binding = G_complex - (G_receptor + G_ligand), where G_receptor denotes the energy of the isolated receptor and G_ligand signifies the energy of the isolated ligand. Alternatively, ΔG_binding equals ΔH - TΔS, with ΔH denoting the binding enthalpy and -TΔS indicating the entropy change arising from conformational alterations upon ligand binding. Without entropy computations, the obtained value approximates the effective free energy, which is suitable for comparative assessment of binding strengths in similar systems. This study determined the effective free energy across the 100 ns duration, utilising 125 frames collected at 80 ps intervals (from 0 to 100 ns). This approach produced an averaged binding energy, illustrating the dynamic aspects of protein-ligand interactions and offering an understanding of affinity and stability in simulated conditions.

As presented in Table 4, the MMGBSA analysis for the CPD5-7E6I and DHEA-7E6I complexes revealed average binding free energies (ΔTOTAL) of –5.13 kcal/mol for CPD5-7E6I and –14.38 kcal/mol for DHEA-7E6I. The components influencing ΔTOTAL include van der Waals interactions (ΔVDWAALS) at –9.71 kcal/mol for CPD5-7E6I and –21.08 kcal/mol for DHEA-7E6I, electrostatic interactions (ΔEEL) at –4.95 kcal/mol and –3.43 kcal/mol, respectively, and solvation contributions (ΔGSOLV) at 9.53 kcal/mol for CPD5-7E6I and 10.13 kcal/mol for DHEA-7E6I. Other components, such as bond, angle, dihedral, and 1-4 interactions, exhibited negligible contributions (0.00 kcal/mol or near zero). The more negative ΔTOTAL for DHEA-7E6I signifies stronger binding affinity and enhanced stability than CPD5-7E6I, primarily driven by favourable van der Waals and electrostatic terms, despite a positive solvation penalty.

Table 4 — Free energy for binding was obtained using MMGBSA calculations

Energy Component	Average (kcal/mol)		Standard Deviation	
	CPD5-7E6I	DHEA-7E6I	CPD5-7E6I	DHEA-7E6I
ΔBOND	0.00	0.00	0.00	0.00
ΔANGLE	–0.00	–0.00	0.00	0.00
ΔDIHED	0.00	0.00	0.00	0.00
ΔUB	0.00	0.00	0.00	0.00
ΔIMP	–0.00	0.00	0.00	0.00
ΔCMAP	0.00	0.00	0.00	0.00
ΔVDWAΔALS	–9.71	–21.08	8.91	5.53
ΔEEL	–4.95	–3.43	6.66	5.51
Δ1-4 VDW	–0.00	0.00	0.00	0.00
Δ1-4 EEL	–0.00	–0.00	0.00	0.00
ΔEGB	10.67	12.73	10.04	5.20
ΔESURF	–1.14	–2.60	1.03	0.69
ΔGGAS	–14.66	–24.51	14.07	8.25
ΔGSOLV	9.53	10.13	9.13	4.80
ΔTOTAL	–5.13	–14.38	5.46	4.88

Quantum chemistry computation using DFT method

Density Functional Theory (DFT) represents a robust computational technique employed to investigate the electronic configuration and reactivity of molecules and materials. This approach aligns calculated outcomes with empirical data, offering substantial understanding of chemical and biological processes. The DFT calculations were executed utilising ORCA 6.1.1 and IboView v20211019. Density functional theory evaluations were performed on CPD5 and DHEA to analyse their interaction potentials with the target enzyme, yielding distinct results as detailed in Table 5.

The energies of the highest occupied molecular orbital (HOMO) and lowest unoccupied molecular orbital (LUMO) provide crucial details about molecular characteristics, chemical reactivity, and interaction modes of these compounds, as depicted in Fig. 8. The HOMO energy reflects the capacity for electron donation, whereas the LUMO energy indicates the potential for electron acceptance. CPD5 displays a lower EHOMO (–10.1463 eV) compared to DHEA (–9.1999 eV), suggesting reduced ease in electron donation and decreased susceptibility to oxidation. Conversely, CPD5 shows a lower LUMO energy (2.8476 eV) than DHEA (3.8576 eV), indicating improved electron-acceptance ability. The energy gap (ΔE) serves as a metric for assessing stability and chemical reactivity, where a narrower gap typically denotes higher reactivity and lower stability, and a wider gap implies greater stability and diminished reactivity[58]. CPD5 presents a ΔE of 12.9939 eV, while DHEA exhibits a ΔE of 13.0575 eV, suggesting that CPD5 possesses slightly higher reactivity and lower stability than DHEA. Ionisation potential (IP), defined as the negative of HOMO energy, quantifies the energy required for electron removal, with higher values denoting increased resistance to oxidation. Electron affinity (EA), approximated as the negative of LUMO energy, evaluates a molecule's electron-accepting capability. Elevated EA values (more negative LUMO energies) reflect stronger electron-gaining tendencies, indicating enhanced electron-acceptor traits[59]. CPD5 exhibits an IP of 10.1463 eV and an EA of –2.8476 eV, whereas DHEA shows an IP of 9.1999 eV and an EA of –3.8576 eV, highlighting DHEA's greater electron-acceptance potential.

Chemical hardness (η), calculated as half the energy gap (η = ΔE/2), measures resistance to

Table 5 — Quantum descriptors of CPD5 and DHEA

Molecule	EHOMO (eV)	ELUMO (eV)	ΔE (eV)	μ (eV)	χ (eV)	η (eV)	σ (eV^{-1})	ω (eV)
CPD5	–10.1463	2.8476	12.9939	–3.6494	3.6494	6.4970	0.1539	1.0249
DHEA	–9.1999	3.8576	13.0575	–2.6712	2.6712	6.5288	0.1532	0.5464

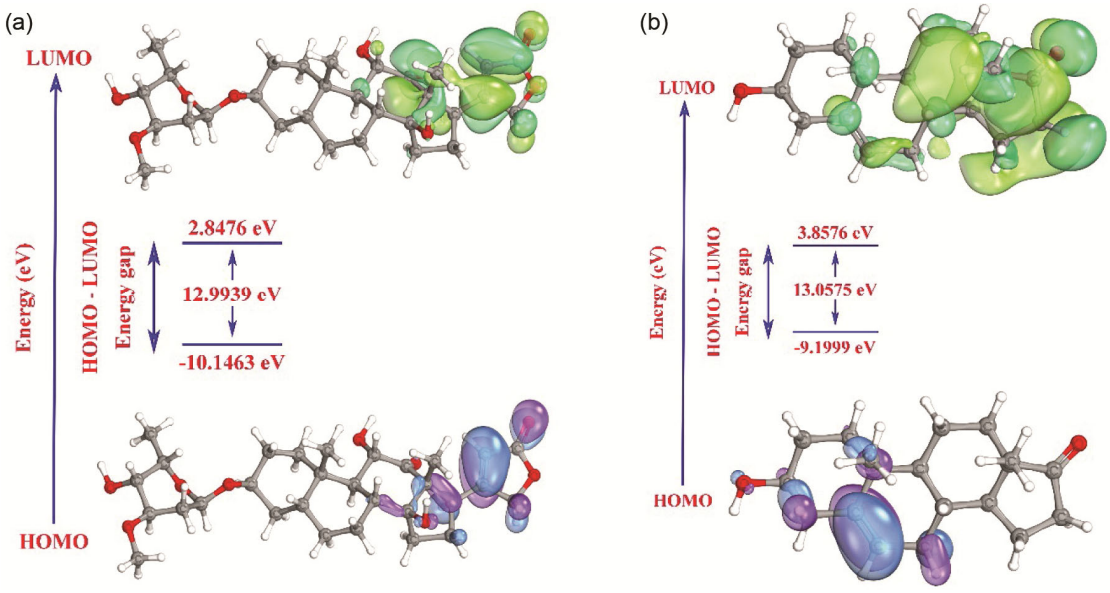

Fig. 8 — HOMO and LUMO surface diagrams of CPD5 (A) and DHEA (B)

changes in electron distribution, while softness (σ), the inverse of hardness (σ = 1/η), indicates predisposition to reactivity[60]. CPD5 demonstrates a hardness of 6.4970 eV and a softness of 0.1539 eV^{-1}, compared to DHEA's hardness of 6.5288 eV and softness of 0.1532 eV^{-1}, implying CPD5 displays marginally greater reactivity. Electronegativity (χ), determined as the average of IP and EA (χ = (IP + EA)/2), assesses the ability to attract electron density. CPD5 achieves a χ of 3.6494 eV, while DHEA attains a χ of 2.6712 eV, signifying CPD5's stronger tendency to draw electrons. Chemical potential (μ), expressed as the negative of electronegativity (μ = -χ), characterises the inclination of a species to acquire or relinquish electrons. More negative chemical potential values signify a stronger preference for electron acquisition[61]. CPD5 exhibits a μ of –3.6494 eV, and DHEA a μ of –2.6712 eV, aligning with CPD5's superior electron-acceptance dominance. The electrophilicity index (ω), computed as $\omega = \mu^2/(2\eta)$, evaluates electrophilic strength, with larger values denoting more pronounced electrophilic behaviour[62]. CPD5 records an ω of 1.0249 eV, whereas DHEA registers 0.5464 eV, suggesting CPD5's enhanced capability for electrophilic interactions with biological targets.

Conclusion

The pharmacokinetics and molecular targets of selected steroids from *Dracaena draco* L. and *Strophanthus divaricatus* as potential anti-gastric cancer agents. The results exhibited that these steroids are likely to induce apoptosis through modulation of key signalling pathways, with G6PD inhibition increasing reactive oxygen species (ROS) and activating caspase-3, while regulating cell survival and proliferation *via* targets such as ATP1A1 and NOTCH1. Molecular docking analyses with the protein 7E6I revealed that CPD5 is more stable and better localised within the 7E6I binding pocket than DHEA. The molecular dynamics simulation further confirmed a consistent binding mode, with stable interactions maintained throughout the 100 ns simulation, as evidenced by RMSD values of 0.35-0.55 nm, Rg values of 1.7-1.8 nm, and dynamic hydrogen bond formations, underscoring CPD5's potential to inhibit 7E6I effectively. MMGBSA results indicated a superior binding free energy for DHEA-7E6I (–14.38 kcal/mol) compared to CPD5-7E6I (–5.13 kcal/mol), supported by favourable van der Waals and electrostatic components despite solvation costs, denoting greater strength. DFT analysis revealed contrasting reactivities, with CPD5 exhibiting reduced HOMO energy (–10.1463 eV) and diminished energy gap (12.9939 eV) *versus* DHEA (–9.1999 eV and 13.0575 eV), implying increased electron-acceptance, reactivity, and electrophilicity (1.0249 eV *vs*. 0.5464 eV). Based on the *in silico* ADMET evaluation results for CPD5 and DHEA, it can be concluded that CPD5 satisfies key pharmacokinetic criteria, demonstrating non-toxicity, superior stability with lower clearance, and high intestinal absorption. As a result, CPD5 shows potential as a future drug for treating gastric cancer by inducing apoptosis through 7E6I inhibition. Furthermore, CPD5 could be a foundation for designing new compounds with enhanced biological activities, improved safety profiles, and novel therapeutic applications in cancer therapy.

Supplementary Information

Supplementary information is available in the website https://nopr.niscpr.res.in/handle/123456789/58776.

Funding

This research is funded by Thai Nguyen University of Education under grant number TNUE-2025-09.

Conflict of Interest

The authors have declared no conflict of interest.

Author's Contributions

The author confirms the sole responsibility for the conception of the study, presented results and manuscript preparation. All data were generated in-house and that no paper mill was used.

References

1 Bray F, Laversanne M, Sung H, Ferlay J, Siegel R L, Soerjomataram I & Jemal A, *CA Cancer J Clin*, 74 (2024) 229.
2 Kumar R, Chaudhary K, Gupta S, Singh H, Kumar S, Gautam A, Kapoor P & Raghava G P S, *Sci Rep*, 3 (2013) 1445.
3 Imtiaz S, Ferdous U T, Nizela A, Hasan A, Shakoor A, Zia A W & Uddin S, *Eur J Med Chem*, 290 (2025) 117535.
4 Tsimberidou A M, *Cancer Chemother Pharmacol*, 76 (2015) 1113.
5 Ke X, & Shen L, *Front Lab Med*, 1 (2017) 69.
6 Yang P L, *Metabolomics and lipidomics: Yet more ways your health ıs ınfluenced by fat*, (Academic Press, Boston) 2016, p. 181.
7 Cappellini M D & Fiorelli G, *Lancet*, 371 (2008) 64.

8 Hamilton N M, Dawson M, Fairweather E E, Hamilton N S, Hitchin J R, James D I, Jones S D, Jordan A M, Lyons A J, Small H F, Thomson G J, Waddell I D & Ogilvie D J, *J Med Chem*, 55 (2012) 4431.

9 Jin X, Li X, Li L, Zhong B, Hong Y, Niu J & Li B, *J Biol Chem*, 298 (2022) 102587.

10 Nakamura M, Magara T, Yoshimitsu M, Kano S, Kato H, Yokota K, Okuda K & Morita A, *J Immunother Cancer*, 12 (2024) e008441.

11 Wang M, Li Y, Pan T & Jia N, *Heliyon*, 10 (2024) e34462.

12 Naeem A, Hu P, Yang M, Zhang J, Liu Y, Zhu W & Zheng Q, *Molecules*, 27 (2022) 8367.

13 AlQathama A, Bader A, Al-Rehaily A, Gibbons S & Prieto J M, *Eur J Integr Med*, 49 (2022) 102083.

14 Sadybekov A V & Katritch V, *Nature*, 616 (2023) 673.

15 Sharma P, Sharma K & Nandave M, *Computational approaches in drug discovery and design*, (Academic Press, Boston) 2023, p. 53.

16 Ran H L, Huang S Z, Wang H, Yang L, Gai C J, Duan R J, Dai H F, Guan Y L & Mei W L, *Phytochemistry*, 210 (2023) 113668.

17 Davis R L, *iScience*, 23 (2020).

18 Keiser M J, Roth B L, Armbruster B N, Ernsberger P, Irwin J J & Shoichet B K, *Nat Biotechnol*, 25 (2007) 197.

19 Greenblatt J F, Alberts B M, & Krogan N J *Cell*, 187 (2024) 6501.

20 Szklarczyk D, Gable A L, Nastou K C, Lyon D, Kirsch R, Pyysalo S, Doncheva N T, Legeay M, Fang T, Bork P, Jensen L J & von Mering C, *Nucleic Acids Res*, 49 (2021) D605.

21 Clarke D J, Kuleshov M V, Schilder B M, Torre D, Duffy M E, Keenan A B, Lachmann A, Feldmann A S, Gundersen G W, Silverstein M C, Wang Z & Ma'ayan A, *Nucleic Acids Res*, 46 (2018) W171.

22 Nguyen H D, *Indian J Chem*, 64 (2025) 383.

23 Vu H H, Jin C & Chang J H, *Biochem Biophys Res Commun*, 553 (2021) 85.

24 Van Der Spoel D, Lindahl E, Hess B, Groenhof G, Mark A E & Berendsen H J C, *J Comput Chem*, 26 (2005) 1701.

25 Guex N & Peitsch M C, *Electrophoresis*, 18 (1997) 2714.

26 Zoete V, Cuendet M A, Grosdidier A & Michielin O, *J Comput Chem*, 32 (2011) 2359.

27 Pires D E V, Blundell T L & Ascher D B, *J Med Chem*, 58 (2015) 4066.

28 Genheden S & Ryde U, *Expert Opin Drug Discov*, 10 (2015) 449.

29 Nyangiwe N N, *Next Mater*, 8 (2025) 100683.

30 Neese F, *WIREs Comput Mol Sci*, 15 (2025) e70019.

31 Knizia G & Klein J E, *Angew Chemie Int Ed*, 54 (2015) 5518.

32 Knizia G, *J Chem Theory Comput*, 9 (2013) 4834.

33 Hanwell M D, Curtis D E, Lonie D C, Vandermeersch T, Zurek E & Hutchison G R, *J Cheminform*, 4 (2012) 17.

34 Luo J, Xue Z Q, Liu W M, Wu J L & Yang Z Q, *J Phys Chem A*, 110 (2006) 12005.

35 Das R, Vigneresse J L & Chattaraj P K, *Int J Quantum Chem*, 114 (2014) 1421.

36 Alves M J, Froufe H J, Costa A F, Santos A F, Oliveira L G, Osório S R, Abreu R M, Pintado M & Ferreira I C, *Molecules*, 19 (2014) 1672.

37 Righetti P G & Boschetti E, *Low-abundance protein access by combinatorial peptide libraries*, (Elsevier, Boston) 2013, p. 79.

38 Bitencourt-Ferreira G, Veit-Acosta M & de Azevedo W F, *Van der Waals potential in protein complexes*, (Springer, New York), 2019, p. 79.

39 Patil R, Das S, Stanley A, Yadav L, Sudhakar A & Varma A K, *PLoS One*, 5 (2010) e12029.

40 Lippert T & Rarey M, *J Cheminform*, 1 (2009) 13.

41 Etebar N, Hamidi S H H, Naderpour S, Abouali O, Hamidi S H H, Hajipour-Verdom B, Zali A, Alipour M & Rahimzadegan M, *Front Mol Biosci*, Volume 11 (2024).

42 Yin J, Bowen D & Southerland W M, *J Mol Graph Model*, 24 (2006) 233.

43 Bagewadi Z K, Yunus Khan T M, Gangadharappa B, Kamalapurkar A, Mohamed Shamsudeen S & Yaraguppi D A, *Saudi J Biol Sci*, 30 (2023) 103753.

44 Li J, Shen J, Li X, Qin Z, Jiang Z, Sun S & Li Z, *J Indian Chem Soc*, 101 (2024) 101478.

45 Zia M, Parveen S, Shafiq N, Rashid M, Farooq A, Dauelbait M, Shahab M, Salamatullah A M, Brogi S & Bourhia M, *ACS Omega*, 9 (2024) 2161.

46 Vrbanac J, & Slauter R, *ADME in drug discovery*, (Academic Press, Boston) 2017, p. 39.

47 Kalantzi L, Goumas K, Kalioras V, Abrahamsson B, Dressman J B & Reppas C, *Pharm Res*, 23 (2006) 165.

48 Berellini G, Springer C, Waters N J & Lombardo F, *J Med Chem*, 52 (2009) 4488.

49 Clark D E, *Computational prediction of blood-brain barrier permeation*, (Academic Press, Boston) 2005, p. 403.

50 Roland N, Fritz S & Helmut E, *Clin Microbiol Rev*, 23 (2010) 858.

51 Omar S A & Webb A J, *J Mol Cell Cardiol*, 73 (2014) 57.

52 Domínguez-Villa F X, Durán-Iturbide N A & Ávila-Zárraga J G, *Bioorg Chem*, 106 (2021) 104497.

53 Nebert D W, Wikvall K & Miller W L, *Philos Trans R Soc B Biol Sci*, 368 (2013) 20120431.

54 5Rodrigues-Junior V S, Villela A D, Abbadi B L, Sperotto N D M, Pissinate K, Picada J N, Bondan da Silva J, Bizarro C V, Machado P & Basso L A, *Regul Toxicol Pharmacol*, 111 (2020) 104553.

55 Li Y, Meng Q, Yang M, Liu D, Hou X, Tang L, Wang X, Lyu Y, Chen X, Liu K, Yu A M, Zuo Z & Bi H, *Acta Pharm Sin B*, 9 (2019) 1113.

56 Blake M J, Castro L, Leeder J S & Kearns G L, *Semin Fetal Neonatal Med*, 10 (2005) 123.

57 Guy R C, *Ames test*, (Academic Press, Oxford) 2024, p. 377.

58 Paneru T R, Chaudhary M K, Tandon P, Chaudhary T & Joshi B D, *Chem Phys Impact*, 8 (2024) 100641.

59 Adindu E A, Godfrey O C, Agwupuye E I, Ekpong B O, Agurokpon D C, Ogbodo S E, Benjamin I & Louis H, *Chem Phys Impact*, 7 (2023) 100296.

60 Kaya S & Kaya C, *Comput Theor Chem*, 1060 (2015) 66.

61 Dong X, Oganov A R, Cui H, Zhou X F & Wang H T, *Proc Natl Acad Sci*, 119 (2022) e2117416119.

62 Azeez Y H, Kareem R O, Qader A F, Omer R A & Ahmed L O, *Next Mater*, 3 (2024) 100184.